# An impact of estimating tropospheric delay gradients on tropospheric delay estimations in the summer using the Japanese nationwide GPS array

Tetsuya Iwabuchi,[1] Shin'ichi Miyazaki,[2] Kosuke Heki,[3] Isao Naito,[4] and Yuki Hatanaka[5]

Received 19 February 2002; revised 22 August 2002; accepted 13 November 2002; published 30 May 2003.

[1] We used various analysis strategies to evaluate zenith tropospheric delays (ZTDs) retrieved from the Japanese nationwide Global Positioning System (GPS) array in the summer of 1996. We compared results from the network solution obtained by daily routine data analyses and two-point positioning analyses with and without a tropospheric delay gradient model. We investigated two 14-day periods in summer 1996, when water vapor distributions were highly azimuthally asymmetric. ZTD differences up to 4 mm, dependent on clusters used in the network analysis, were found between the network and the point analyses. We also found that differences in the estimated ZTD between the two-point positioning analyses were correlated with the north components of the estimated tropospheric delay gradients. This is consistent with our simulation studies based on the north-south asymmetry in the satellite coverage. The estimated tropospheric delay gradient vectors averaged over the periods pointed southward, which matches with the general meteorological condition in summer over the Japanese Islands. The temporal and spatial variations in the gradient estimates matched well with the moisture field determined by ZTD, in particular, during the passage of a weather front. Thus, tropospheric delay gradients obtained by GPS are expected to contain real horizontally anisotropic distribution of water vapor. *INDEX TERMS:* 0394 Atmospheric Composition and Structure: Instruments and techniques; 1294 Geodesy and Gravity: Instruments and techniques; 3354 Meteorology and Atmospheric Dynamics: Precipitation (1854); 3360 Meteorology and Atmospheric Dynamics: Remote sensing; 6904 Radio Science: Atmospheric; *KEYWORDS:* GPS, tropospheric delay, tropospheric delay gradient, GEONET

**Citation:** Iwabuchi, T., S. Miyazaki, K. Heki, I. Naito, and Y. Hatanaka, An impact of estimating tropospheric delay gradients on tropospheric delay estimations in the summer using the Japanese nationwide GPS array, *J. Geophys. Res.*, *108*(D10), 4315, doi:10.1029/2002JD002214, 2003.

## 1. Introduction

[2] The Global Positioning System (GPS) is now widely used as valuable sensors for atmospheric sounding. The sounding methods are mainly divided into two types, GPS radio occultation methods [e.g., *Ware et al.*, 1996] and ground-based observation methods [e.g., *Businger et al.*, 1996]. Both use atmospheric delay, delay of the microwave signal transmitted from the GPS satellite passing through the atmosphere. This paper deals with the ground-based observation method, which is called "ground-based GPS meteorology."

[3] The tropospheric delay (TD) provides information on the amount of water vapor integrated over the path between a GPS satellite and a receiver. We can generally observe more than four or five satellites in the sky at any given time. The delay in the zenith direction, i.e., the zenith tropospheric delay (ZTD), is estimated in GPS analyses using mapping function $M(\theta)$ expressed as

$$TD = M(\theta)ZTD, \tag{1}$$

showing the ratio of the line-of-sight delays to ZTD (see *Davis et al.* [1985] for details), where $\theta$ is the elevation angle of the GPS satellite. In the first approximation, assuming a flat Earth surface, mapping functions are written as

$$M(\theta) = 1/\sin(\theta). \tag{2}$$

Precipitable water vapor (PWV) can be obtained by separating zenith delay due to water vapor (zenith wet delay, ZWD) from the total ZTD and by multiplying the ZWD by a proportional coefficient equal to about 0.15 [e.g., *Hogg et al.*, 1981; *Askne and Nordius*, 1987; *Bevis et al.*, 1992]. Meteorological application studies of the ZTD or

[1]Meteorological Research Institute, Tsukuba, Japan.
[2]Earthquake Research Institute, University of Tokyo, Tokyo, Japan.
[3]National Astronomical Observatory, Mizusawa, Japan.
[4]National Astronomical Observatory, Mitaka, Japan.
[5]Geographical Survey Institute, Tsukuba, Japan.


0148-0227/03/2002JD002214$09.00

PWV obtained by GPS are referred to as ground-based GPS meteorology [e.g., *Businger et al.*, 1996; *Kuo et al.*, 1996; *Ware et al.*, 2000; *Pondeca and Zou*, 2001]. In Japan, a nationwide GPS network, called GPS Earth Observing Network (GEONET), is operated by the Geographical Survey Institute (GSI) to monitor crustal deformation over the Japanese Islands. The network has grown from 610 sites in 1996 to about 1000 now. ZTD for each site is estimated every 3 hours by automatic routine data processing. A project was under way in Japan [*Naito et al.*, 1998; *Tsuda et al.*, 1998] to allow the PWV information provided by GEONET to assimilate into the numerical weather prediction work performed by the Japan Meteorological Agency (JMA).

[4] To evaluate accuracies of the ZTD or PWV by GPS, *Rocken et al.* [1993, 1995] and *Duan et al.* [1996] compared PWV obtained by relative positioning methods of GPS with those observed by water vapor radiometers and radiosondes, and reported that they agreed within 1.5 mm. In GEONET, *Iwabuchi et al.* [2000] showed the possibility of the network as a PWV sensor, which is useful in all weather conditions over the Japanese Islands, by visualizing the two-dimensional PWV distributions obtained by routine network analysis during a front passage that brought a heavy rainfall in the late summer of 1996. In their analyses, the GEONET PWVs were found to be about 3 mm smaller, or drier, than those from the numerical weather prediction data by JMA. *Ohtani and Naito* [2000] also showed that the GEONET PWV in the routine network analysis is negatively biased by about 3 mm from radiosonde observations by JMA. Recently, *Hatanaka et al.* [2001a, 2001b] showed that radomes covering the GPS antennas of GEONET alter the original phase center variation (PCV) pattern of the antenna. They showed that biases in position estimates of earlier GSI network analysis using IGS_01 antenna model (International GPS service, http://igscb.jpl.nasa.gov/) increase with baseline length. New elevation dependent antenna models were empirically derived according to the radome, monument, and antenna types. Hereafter, we call it GEONET PCV model. M. Nishimura et al. (Recomparison of GPS retrieved precipitable water vapor with radiosonde observations, submitted to *Tenki Tokyo*, 2002) have confirmed that the biases between GPS PWVs and PWVs based on the nationwide radiosonde observation network of 14 sites operated by the Japan Meteorological Agency are reduced to about 1 mm in analysis of GEONET with the GEONET PCV model, which has been used for the last 2 years. The remaining biases depend on antenna, radome, and monument types.

[5] The classic IGS_01 PCV model in GSI routine analysis has been replaced with the newly developed GEONET PCV model since 1999. In relative positioning methods, however, a network should span more than a few thousand kilometers to enable estimations of absolute tropospheric delays [e.g., *Duan et al.*, 1996]. Since the new routine network analysis uses data of GEONET that spans about 1500 km, which may be enough to retrieve absolute ZTD but applies a complicated cluster analysis method explained in the next section, the GEONET ZTDs may have a bias coming from intersite correlations of site-specific tropospheric parameters such as pressure, temperature and humidity fields. Such routine analysis ZTDs can be evaluated by comparing them with those from precise point positioning techniques (hereafter called "point analysis").

[6] Apart from the above issue, there are various sources of ZTD biases such as errors in the mapping functions in low elevations [*Niell*, 1996; *Tregoning et al.*, 1998], azimuthal asymmetry of water vapor distribution [*Bar-Sever et al.*, 1998], insufficient modeling of the elevation and/or azimuth dependence of the antenna phase center including the individual difference in the same type of antenna [*Schupler et al.*, 1994; *Fang et al.*, 1998], and multipath [*Elosegui et al.*, 1995; *Georgiadou and Kleusberg*, 1998]. The ZTD bias caused by errors in the mapping functions are negligible in the case of GEONET because GEONET sites do not observe elevations lower than 15°. The ZTD biases caused by multipath will be discussed in another paper (T. Iwabuchi et al., Tsukuba GPS Dense Net Campaign Observation: Comparison of stacking maps of slant tropospheric delay residuals estimated in three types of software, submitted to *Journal of the Meteorological Society of Japan*, 2003).

[7] Accordingly, among the bias sources, we focus on the influence of tropospheric gradients on the ZTD accuracy. We first evaluate it by comparing ZTDs estimated with different strategies. A very humid summer in Japan would be ideal for such a study. We select two periods in the 1996 summer, and perform two-point positionings with and without a tropospheric delay gradient model. We first compare different ZTD estimates between the routine network analysis and point analysis both without a tropospheric delay gradient model. Second, we investigate the ZTD difference between point analyses with and without a tropospheric delay gradient model to study the effect of estimating the gradients. We finally investigate the meteorological reality of the estimated tropospheric delay gradients. The improvement in site coordinate repeatability by modeling tropospheric delay gradients is reported using the same data sets in a separate paper [*Miyazaki et al.*, 2003].

## 2. Data and Analyses

### 2.1. Analysis Period and GPS Data

[8] We studied two periods in summer, the most humid season in Japan. A period from 16 July to 29 July 1996, is in the rainy season, and a period B from 28 August to 10 September 1996 (UTC), is at the end of summer when humid and dry atmospheres alternate frequently as weather fronts move over Japan. Hereafter, we call the former and latter periods Period A and Period B, respectively. Highly uneven water vapor distributions provide a suitable situation to study the influences of tropospheric delay gradients on GPS data analyses. Out of these periods, we select two days for case studies when large tropospheric delay gradients are expected. On 20 July, a tropical cyclone stayed over Central Japan, and on 1 September, a weather front crossed Japan from West to East. Hereafter, we call these two days, Case I and Case II, respectively. Figure 1 shows the weather conditions at 0000 UTC on the two days. The PWV distribution shown by *Iwabuchi et al.* [2000] for Case II suggests the existence of remarkable azimuthal asymmetry of water vapor distributions on both sides of the weather front.

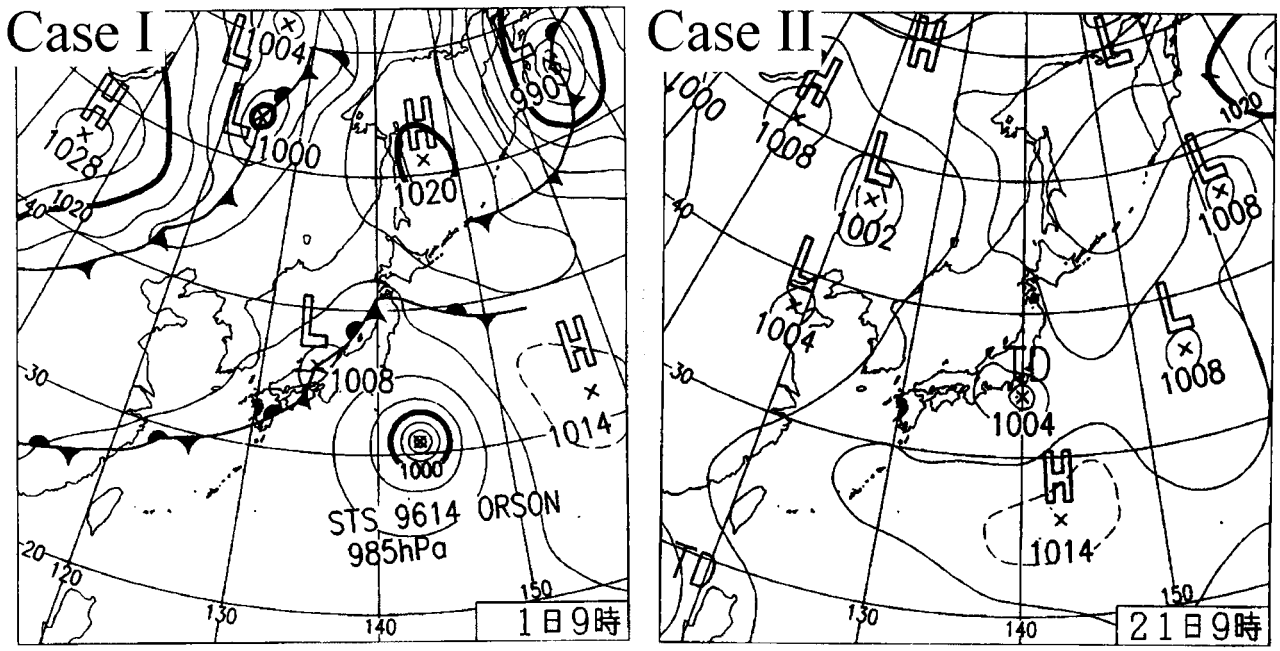


**Figure 1.** Weather maps at 00 (UTC) of Case I, 20 July, and Case II, 1 September 1996 (courtesy of the Japan Meteorological Agency). The two maps show that a stationary tropical cyclone stayed over Central Japan on 20 July (Case I) and a weather front moved eastward over the Japanese Islands on 1 September (Case II), respectively.

[9] We use GEONET data and ZTD solutions from the new GSI's routine network analysis with the GEONET PCV model for the two periods (Period A and Period B). In this section, we give the details of the routine network analysis strategy and of our analyses. In 1996, GEONET consisted of 610 sites with three different receiver-antenna types, 110 sites in the Kanto-Tokai area equipped with Trimble 4000 SSE, 100 sites in the whole nation equipped with Ashtech Z-XIII, and the rest equipped with Trimble 4000 SSI. Those stations started operations in April 1994, October 1994, and April 1996, respectively [*Miyazaki et al.*, 1997] (see also Plate 1 of *Iwabuchi et al.* [2000], for site distributions). GEONET stations continuously record dual-frequency phases every 30 s from GPS satellites at elevations higher than 15°. The data are transmitted to GSI through public telephone lines once a day.

### 2.2. Routine Network Analysis by GSI

[10] The routine network analysis for GEONET data is performed at GSI using the Bernese GPS software ver. 4.2 (hereafter, Bernese) [*Rothacher and Mervart*, 1996]. Bernese performs "double differences" as basic observables for processing. First, data from GPS carrier phase observation at a receiver from one GPS satellite are subtracted from that at other receivers at the same time. It is called "single difference," which is free from the common satellite-clock error, and then, double difference is performed by subtracting the single difference from other single differences made by other GPS satellites. By using the double difference, receiver and satellite clock errors are canceled completely.

[11] Table 1 shows details of the setting of the parameters for the routine network analyses. The precise orbit information and the Earth rotation parameters, provided by the IGS, are used. Periodic variations of site coordinates due to ocean tidal loading, which cause ZTD biases in sites which are located near the ocean, like the Japanese Islands [*Hatanaka et al.*, 2001c], are corrected in this analysis using model GOTIC2 [*Matsumoto et al.*, 2001]. The mapping function in equation (1) used by them is Niell's dry and wet mapping function (NMF) [*Niell*, 1996] for the azimuthally isotropic delay.

[12] GEONET is divided into two subnetworks based on antenna-receiver types, i.e., Trimble subnetwork of 510 sites and Ashtech subnetwork of 100 sites. To retrieve absolute and precise ZTD, analysis with a nationwide network in each subnetwork is desirable because the network has a span large enough to decorrelate site-specific tropospheric parameters. However, assigned memory size and speed in network analyses roughly in proportion to the second power of the number of stations, i.e., (the number of station)$^2$, and thus these two subnetworks are further

**Table 1.** Analysis Strategies for Net in GSI, No-Grad, and Grad Showing Precise Point Analyses With and Without Tropospheric Delay Gradient Model in This Study[a]

| | | ZTD Estimation | | Gradient Estimation | |
|---|---|---|---|---|---|
| Strategy | Orbit | Method | Interval | Method | Interval |
| Net | IGS | deterministic | 3 hours | no | – |
| No-grad | JPL*[b] | stochastic*[c] | 5 min | no | – |
| Grad | JPL*[b] | stochastic*[c] | 5 min | stochastic*[d] | 5 min |

[a]Net, routine network solution; No-grad, no-gradient point solution; Grad, gradient point solution.
[b]Precise fiducial-free orbit and transformation parameter provided by JPL are used.
[c]Random walk with $\tau = 5.0 \times 10^{-8}$ km/$\sqrt{s}$.
[d]Random walk with $\tau = 5.0 \times 10^{-9}$ km/$\sqrt{s}$.

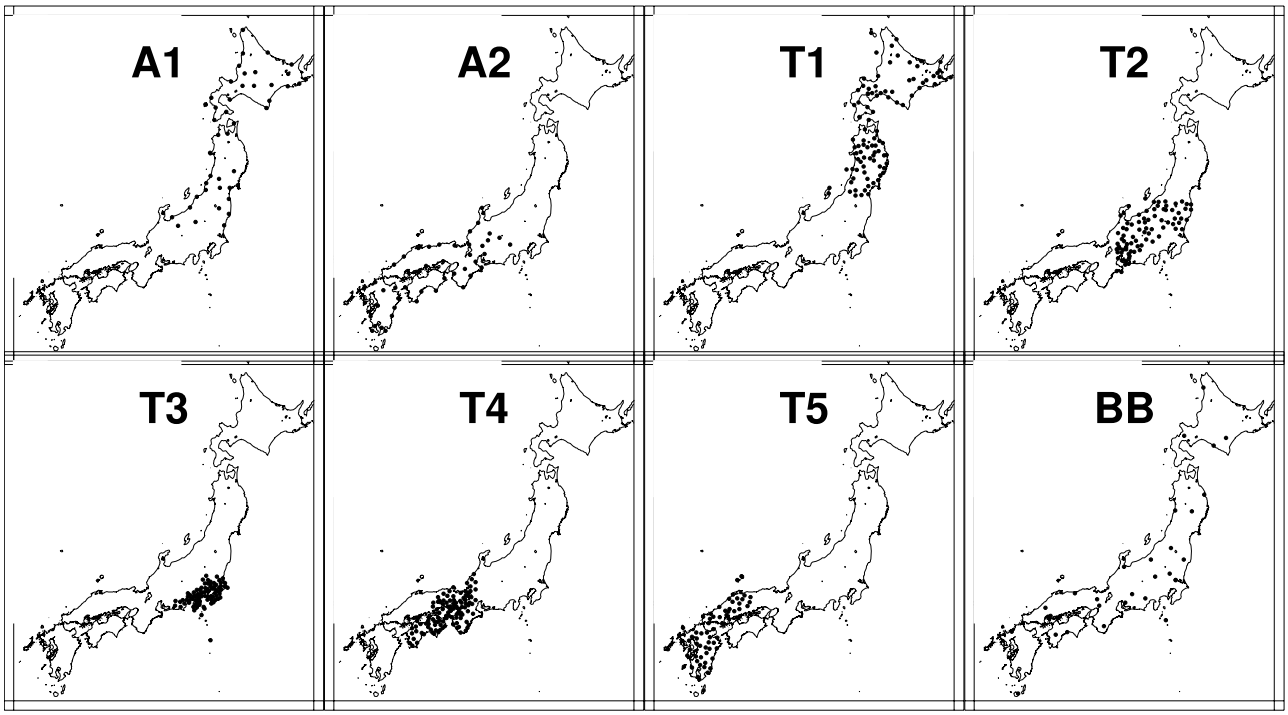


**Figure 2.** Distributions of GPS sites which belong to eight types of clusters in the routine network analysis by Geographical Survey Institute (GSI), where clusters mean networks analyzed simultaneously. A1 and A2 show two Ashtech clusters, T1, T2, T3, T4, and T5 show five Trimble clusters, and BB shows the backbone cluster distributed nationwide analyzed with each Ashtech and Trimble cluster. Also, see Table 2 for antenna and radome types corresponding to each cluster.

divided into regional clusters to analyze faster. The Ashtech network is divided into two regional clusters depicted in A1 and A2 of Figure 2 and the Trimble network is further divided into five regional clusters depicted in T1, T2, T3, T4, and T5 of Figure 2. The span of regional clusters in the Trimble subnetwork is as large as a few hundred kilometers. It is not large enough to obtain absolute ZTD accurately and a larger span in a network is needed to get a more accurate ZTD in relative positioning technique [e.g., *Duan et al.*, 1996]. In the routine network analysis they hence use the "backbone" cluster composed of about 20 sites shown as BB in Figure 2 taken from the whole Trimble subnetwork, where the backbone cluster has a span of about 1500 km. ZTD is estimated every 3 hours at each site, and the regional cluster ZTDs are converted to more accurate ones by combining them with those from the backbone cluster. Consequently, they estimate ZTD five times for the sites in the backbone cluster in the Trimble network and thus five ZTD solutions exist for those sites [*Miyazaki et al.*, 1997; *Miyazaki and Heki*, 2001]. Since the routine analysis is carried out by so-called network analysis, which is based on the relative positioning technique, we call it "network solution."

### 2.3. Point Analysis in This Study

[13] We reanalyzed GEONET data in the same periods with the precise point positioning (PPP) technique using the GIPSY-OASIS II software developed by the Jet Propulsion Laboratory (JPL) (Release 2.6) [*Zumberge et al.*, 1997]. PPP can directly solve receiver clock error along with other parameters by using the sophisticated stochastic filtering technique with precise satellite orbit and satellite clock error information. It is thus not necessary to form double differences to eliminate receiver and satellite clock errors. Since parameters are estimated site by site in PPP, biases of the ZTDs, when the nationwide network is divided into several clusters in the network solution, could be examined by comparing them with those by PPP.

[14] The estimated parameters in PPP, however, strongly depend on the clock error information and the quality of "global parameter" such as satellite orbits, Earth orientation parameters, and reference frame. The errors may introduce biases on position and tropospheric delay estimates while the network solution using a double difference approach can eliminate clock error completely and decrease common errors of global parameter. Further examination with longer data sets is needed to evaluate errors in ZTD estimates caused by such factors.

[15] GIPSY uses a Kalman filtering technique to make time-dependent parameters, such as the ZTD. The tropospheric delay was modeled as a random walk process with the scale parameter $5.0 \times 10^{-8}$ km/$\sqrt{(s)}$, following *Bar-Sever et al.* [1998]. The site positions are estimated daily, but ZTDs are estimated every 5 min. In the analyses, we used precise fiducial-free orbits and satellite clocks, provided by the JPL. The analysis strategy is summarized in Table 1.

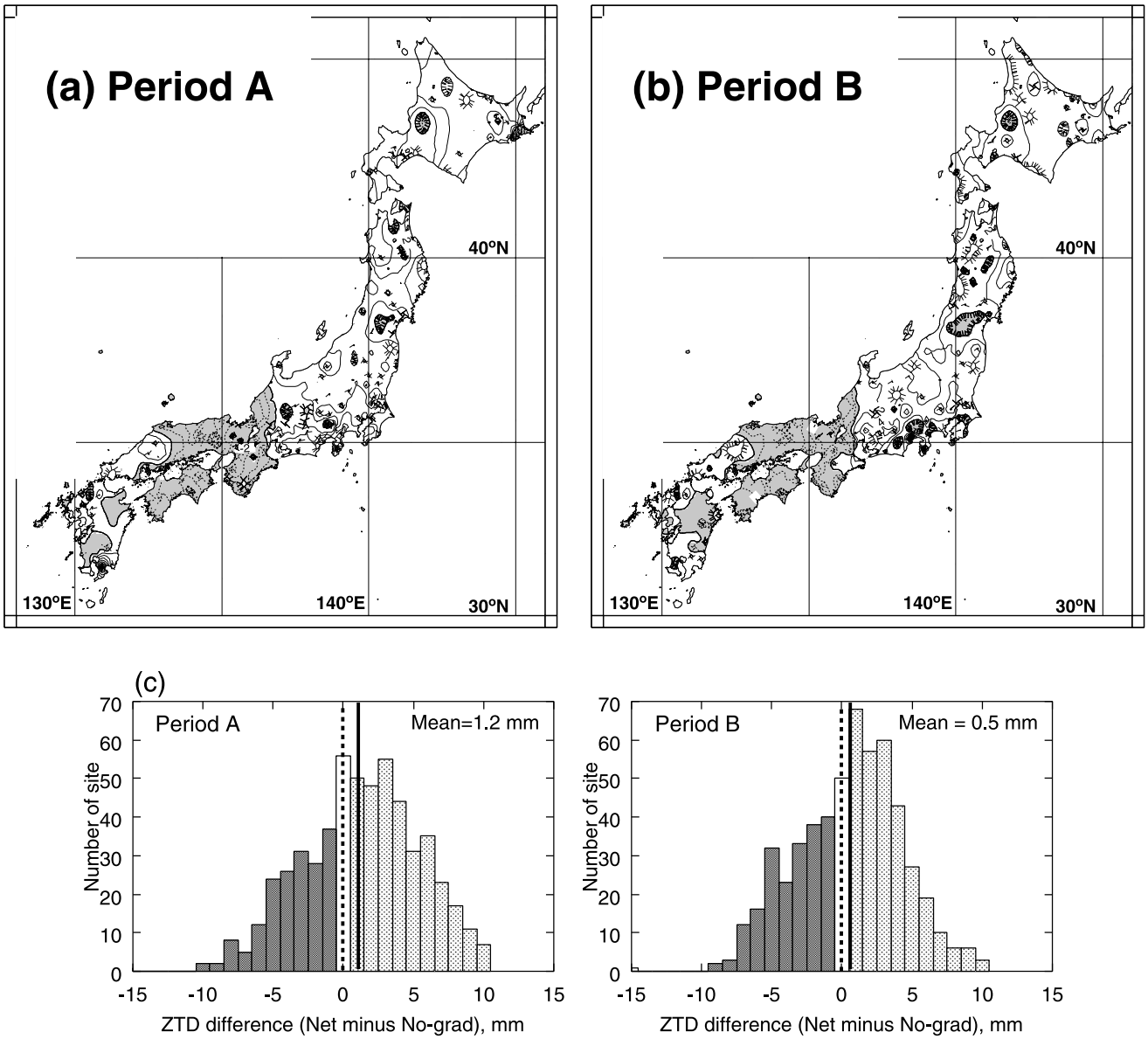


**Figure 3.** The distribution maps of ZTD differences by subtracting ZTD in Net from ZTD in No-grad averaged for the two periods: (a) Period A from 16 July to 29 July 1996 (UTC), (b) Period B from 28 August to 10 September 1996 (UTC), respectively. The histograms (c) show the distribution of the ZTD differences. Positive and negative values are shown with solid and dashed lines with gray shadow, respectively, with contour interval of 2 mm. The thick contour line shows 0 mm.

[16] We performed two analyses, i.e., with and without a tropospheric delay gradient model [*MacMillan*, 1995] expressed as

$$\Delta TD = M(\theta)\cot\theta[G_E \sin\phi + G_N \cos\phi], \quad (3)$$

where $\phi$ is the azimuth angle measured clockwise from the north. In the analysis with tropospheric delay gradient model, TD is modeled as the sum of isotropic mapping function in equation (1) and anisotropic mapping function in equation (2) as

$$TD = M(\theta)ZTD + M(\theta)\cot\theta[G_E \sin\phi + G_N \cos\phi], \quad (4)$$

where ZTD and gradient vector $\mathbf{G} = (G_N, G_E)$ are estimated simultaneously. The tropospheric delay gradient was also modeled as a random walk process with the scale parameter $5.0 \times 10^{-9}$ km/$\sqrt{(s)}$, following *Bar-Sever et al.* [1998]. Although the elevation cutoff angles of 5° to 7° are recommended to separate isotropic and anisotropic tropospheric delay components [*MacMillan*, 1995; *Bar-Sever et al.*, 1998], we used a cutoff angle of 15°, the upper limit to separate them [e.g., *Beutler et al.*, 2000], simply because of the lack of lower elevation data from GEONET. Mapping function and the ocean loading correction used in the two analyses are the same as those in the routine network analyses. Hereafter, we call the solutions by PPP with and

**Table 2.** Mean ZTD Differences[a]

| Cluster | | A1 | A2 | T1 | T2 | T3 | T4 | T5 | |
|---|---|---|---|---|---|---|---|---|---|
| Antenna Type | | TOP700779A | | TRM23903.00 | | | | | |
| Radome Type | All | GSI3 | GSI3 | GSI4 | GSI4 | GSI1,2 | GSI4 | GSI4 | BB |
| Period A | 1.2 | 1.5 | −0.8 | 3.4 | 2.4 | 4.9 | −3.7 | 0.7 | 3.1 |
| Period B | 0.5 | 3.3 | −0.5 | 1.5 | 3.6 | 1.3 | −3.9 | 0.1 | 2.0 |

[a]Mean ZTD differences were obtained by subtracting ZTD in No-grad from ZTD in Net (Net minus No-Grad) during two periods (Period A and Period B) for all the sites (All) and each cluster in the routine network analysis. See Figure 2 for spatial distributions of cluster definition.

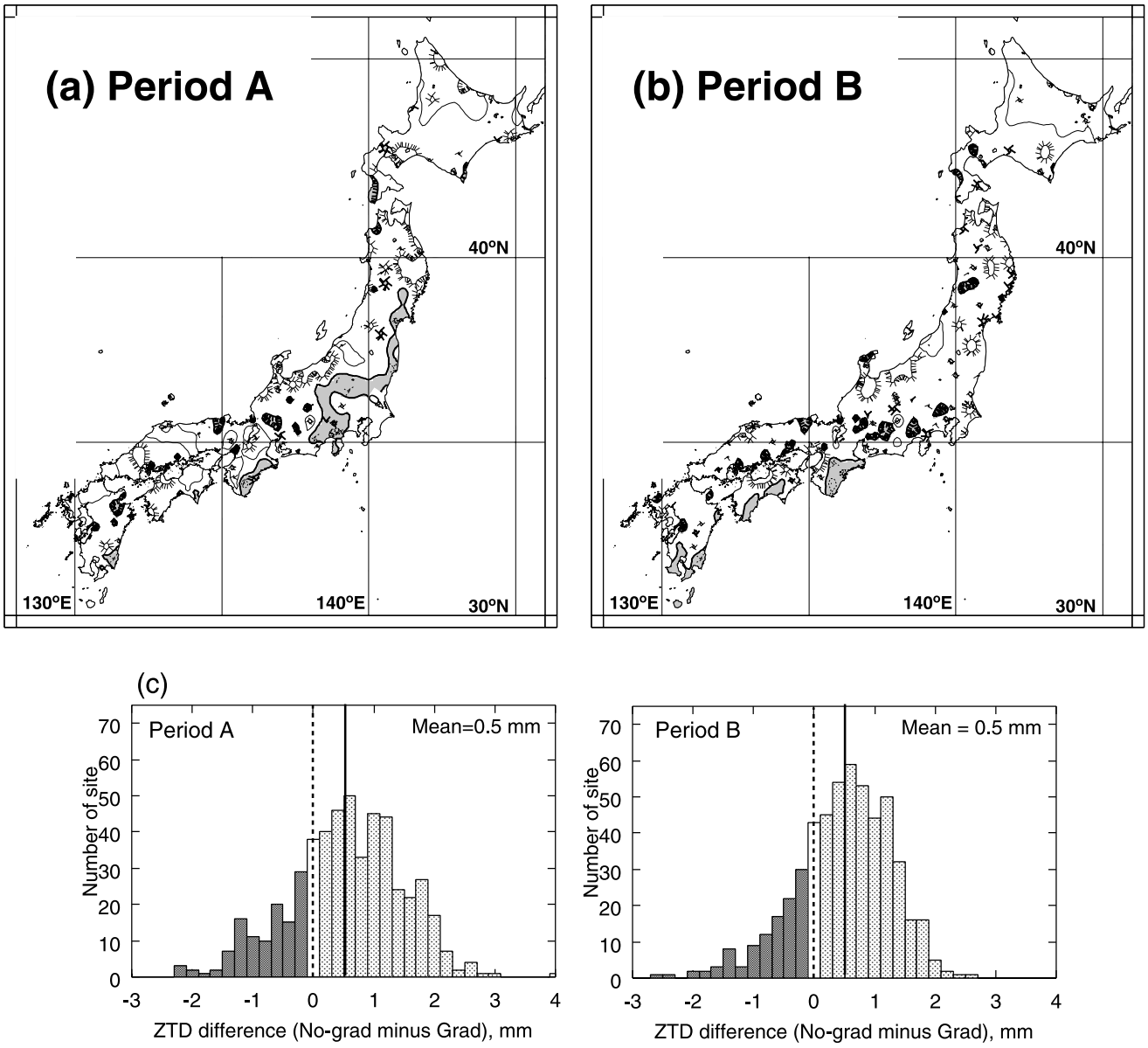


**Figure 4.** The spatial distribution of ZTD differences by subtracting ZTD in the gradient point solution from ZTD in the no-gradient point solution (No-grad minus Grad) averaged for the two periods, (a) Period A and (b) Period B. (c) The histograms showing the distribution of the ZTD differences for Period A (left) and Period B (right). The same maps but averaged for one day in the two cases, (d) Case I and (e) Case II. Positive and negative values are shown with solid and dashed lines with gray shadow in the maps, respectively, with contour interval of 1 mm. The thick contour line shows 0 mm.

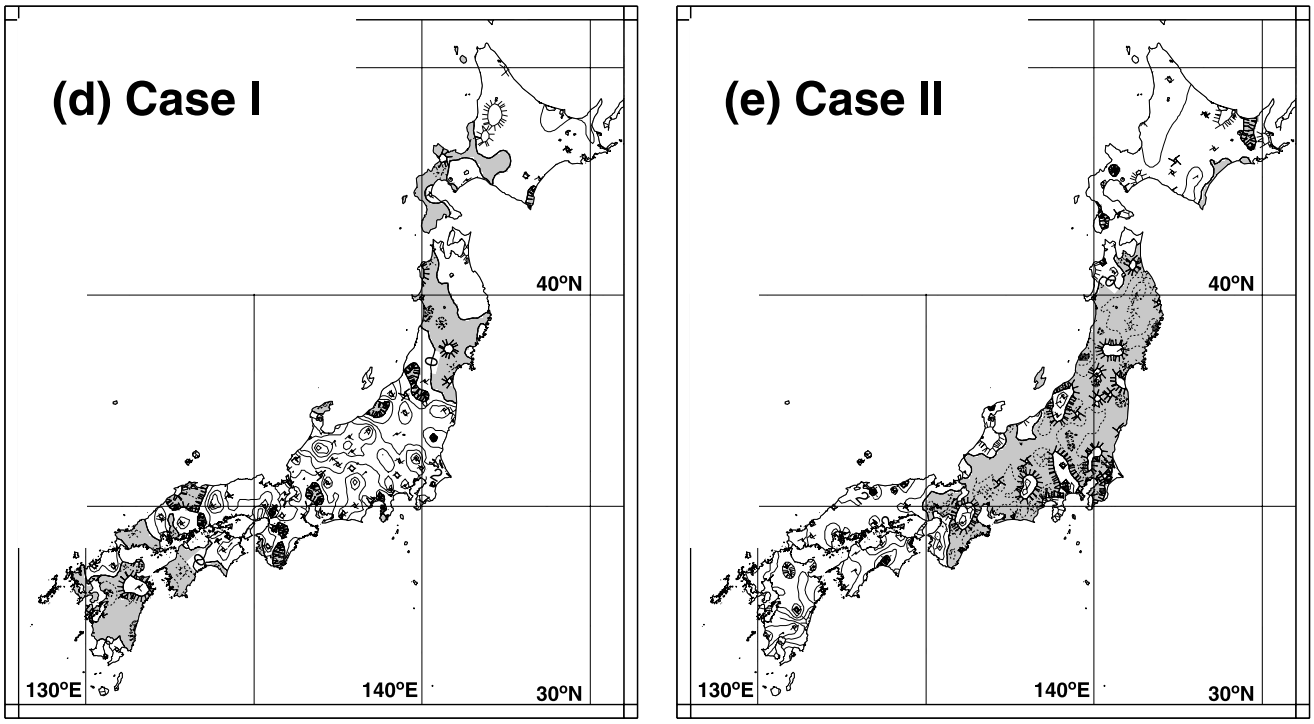


**Figure 4.** (continued)

without the tropospheric delay gradient model as "no-gradient and gradient point solution," respectively. We define abbreviations for the three types of ZTDs, "Net" for network solution, "No-grad" for no-gradient point solution, and "Grad" for gradient point solution.

## 3. Results and Discussions

### 3.1. ZTD Difference Between Network and Point Solutions

[17] Figure 3 shows distribution of averaged ZTD differences between Net and No-grad (i.e., network solution minus no-gradient point solution) over the intervals of Period A and Period B. Both figures are fairly similar despite the period being different. The positive regions in the ZTD differences are distributed in the northeastern part of the Japanese Islands and the negative regions are distributed in the southwestern part. The patterns seem to correspond with those of the cluster shown in Figure 2. One of the significant differences between Period A and Period B is the magnitude of the ZTD differences depicted by contour lines. The magnitude in Period B is smaller than that in Period A.

[18] The histograms in Figure 3c show the ZTD differences between Net and No-grad for Period A and Period B. The average of the difference is about 1.2 and 0.5 mm in Period A and Period B, respectively (the differences actually range from −10 mm to 10 mm). These numbers suggest that ZTD in Net is a little systematically greater (wetter) than those in the No-grad. The right-hand histogram in Figure 3c also shows the ZTD differences distribution near 0. Since the mean ZTD and variability of ZTD in Period B is smaller than that in Period A, the ZTD differences may depend on the total amount of water vapor and temporal variability of water vapor in the atmosphere.

[19] Table 2 summarizes the mean ZTD differences during the two periods. It is evident that there are systematic biases between two solutions and that the biases depend on the cluster. By comparing Table 2 and Figure 2, we notice the biases tend to depend on latitude and longitude. For example, in the case of clusters that belong to the Ashtech subnetwork, the A1 cluster shows positive ZTD differences, while the A2 cluster shows negative ZTD differences. Also, in the case of clusters that belong to the Trimble subnetwork, the T1, T2, and T3 clusters show positive ZTD differences, while the T4 and a part of T5 cluster show negative ZTD differences. Because two analyses use almost the same models, the ZTD differences between Net and No-grad seem to reflect ZTD biases in Net. As mentioned earlier, each cluster is combined with a backbone network. One of the probable causes is that biases and distortion errors of the backbone cluster would be mapped onto ZTD estimates. Further examinations with longer data set are needed to find the cause of the systematic distribution of the ZTD differences. Also, analyses applying several types of completely independent backbone configuration will be needed to reveal the cause of the ZTD differences.

[20] Patterns of ZTD differences in Case I and Case II (daily mean, not shown here) basically show similar patterns in the regional cluster scale (a few hundred kilometers) with those averaged for the two periods in Figure 3. There are some differences in the smaller scale of less than 100 km, suggesting that ZTD differences also depend on weather conditions in each case. The difference may come from the

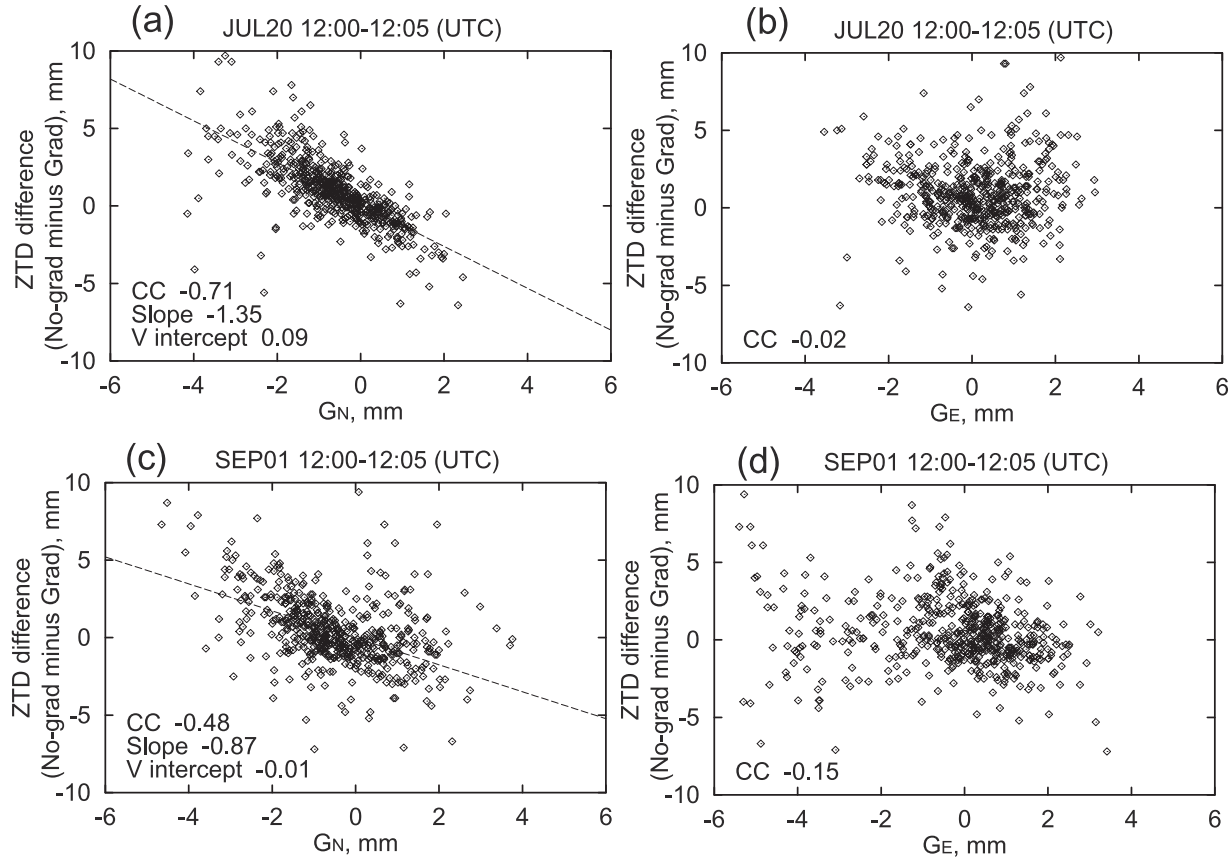


**Figure 5.** Correlation diagrams between magnitude of tropospheric delay gradient vector in Grad and ZTD differences by subtracting ZTD in Grad from ZTD in No-grad (No-grad minus Grad) from 1200 to 1205 UTC in Case I (top figures) and Case II (bottom figures) for the north (left figures) and east (right figures) components. The horizontal and vertical axes show the magnitude of the tropospheric delay gradient vectors ($G_N$, $G_E$) and the ZTD differences respectively. The correlation coefficients (CC) between the magnitude of the vectors and the ZTD differences are displayed in the figure. The estimated slopes and vertical intercepts (V intercept) in linear regression in the north component are also displayed.

difference of interval in ZTD estimation between the two analyses (3 hours in Net and 5 min in No-grad).

### 3.2. ZTD Difference Between No-Gradient and Gradient Point Solutions

[21] Since we use the isotropic mapping function in Net, anisotropic tropospheric delays would give rise to systematic ZTD biases. In the companion paper [*Iwabuchi et al.*, 2003], we showed that the wrongly assuming isotropic tropospheric delay causes errors in both north and vertical site coordinates. We here compare ZTD estimates in No-grad and Grad. Figure 4 shows the averaged pattern of the ZTD differences between the two solutions (No-grad minus Grad) in the two periods (Period A and Period B). The differences are more systematic than those between Net and No-grad though the magnitude of the difference is smaller. The histograms in Figure 4c show positive biases of 0.5 mm on an average for both of the periods; they range from −3 mm to 4 mm. This indicates that the ZTDs in the No-grad tend to be greater than those in the Grad, and the range of the differences is only one third of those between the Net and No-grad (Figure 3).

[22] Figures 4d and 4e show the ZTD differences (No-grad minus Grad) averaged over 20 July 1996, and 1 September 1996, respectively. The ZTD differences are relatively smaller where the estimated ZTD show regional maxima and minima around the tropical cyclone and the front, that is, around the regional extremum of the ZTD distribution. Systematic ZTD differences are significant there, but differ from the distribution patterns of receiver-antenna types roughly divided into three: (1) A1 and A2, (2) T1, T2, T4, and T5, and (3) T3 in Figure 2 (also see Table 2). The patterns in Figures 4d and 4e seem to have typical scales of several hundred kilometers corresponding to weather conditions in the synoptic scale and to depend on the estimated tropospheric delay gradients. Figure 5 shows the correlation between the components of the gradient vectors and the ZTD differences at 12:00–12:05. The correlation between the north gradient and the ZTD difference is significant, −0.71 and −0.48 for Case I and Case II, respectively. We confirmed existence of a similar trend throughout both Period A and Period B.

[23] On the other hand, we can also see site-specific characteristics in the ZTD differences (No-grad minus Grad). In Figure 6, we show the variations of the daily averages of the ZTD differences during the two periods. Although the ZTD differences are at the level of about 1 mm,

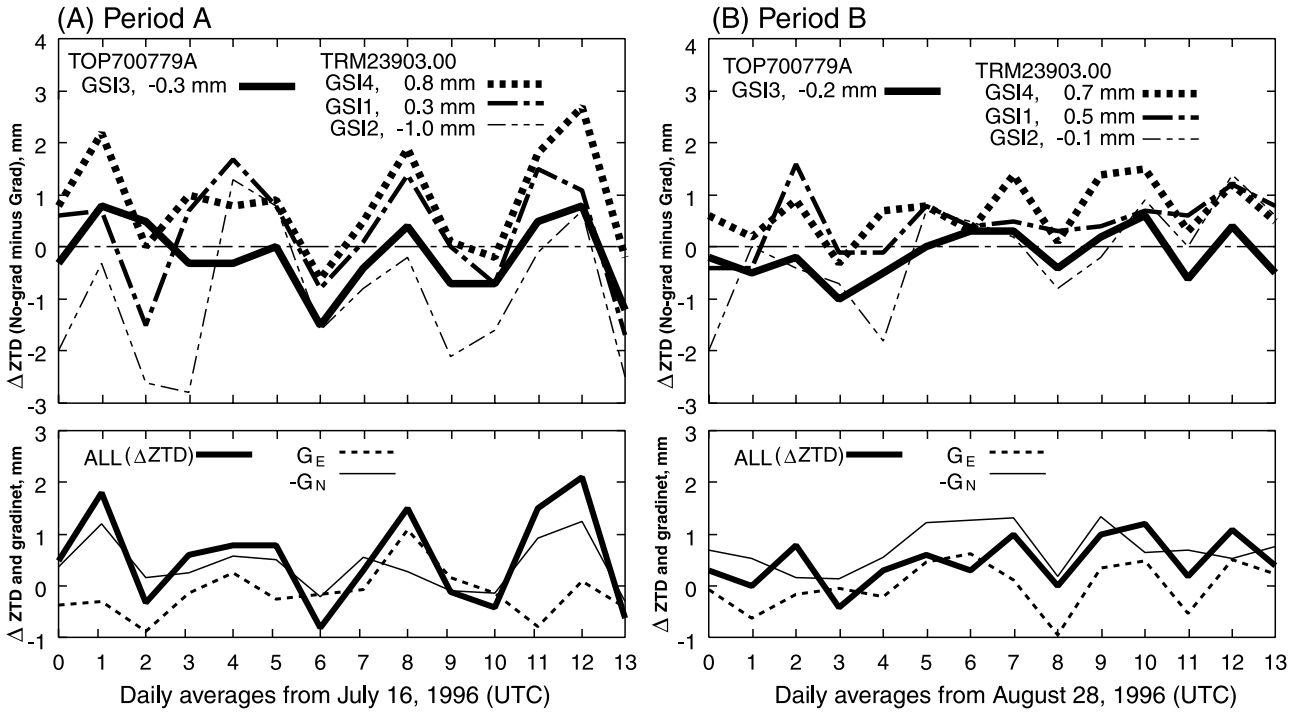


**Figure 6.** The daily ZTD differences between No-grad and Grad (No-grad minus Grad) during two periods, (a) Period A and (b) Period B, for each antenna-radome type (upper panels, see Table 2). The daily averages of $G_E$ and $G_N$ for all sites are plotted with those of ZTD differences (All, lower panels).

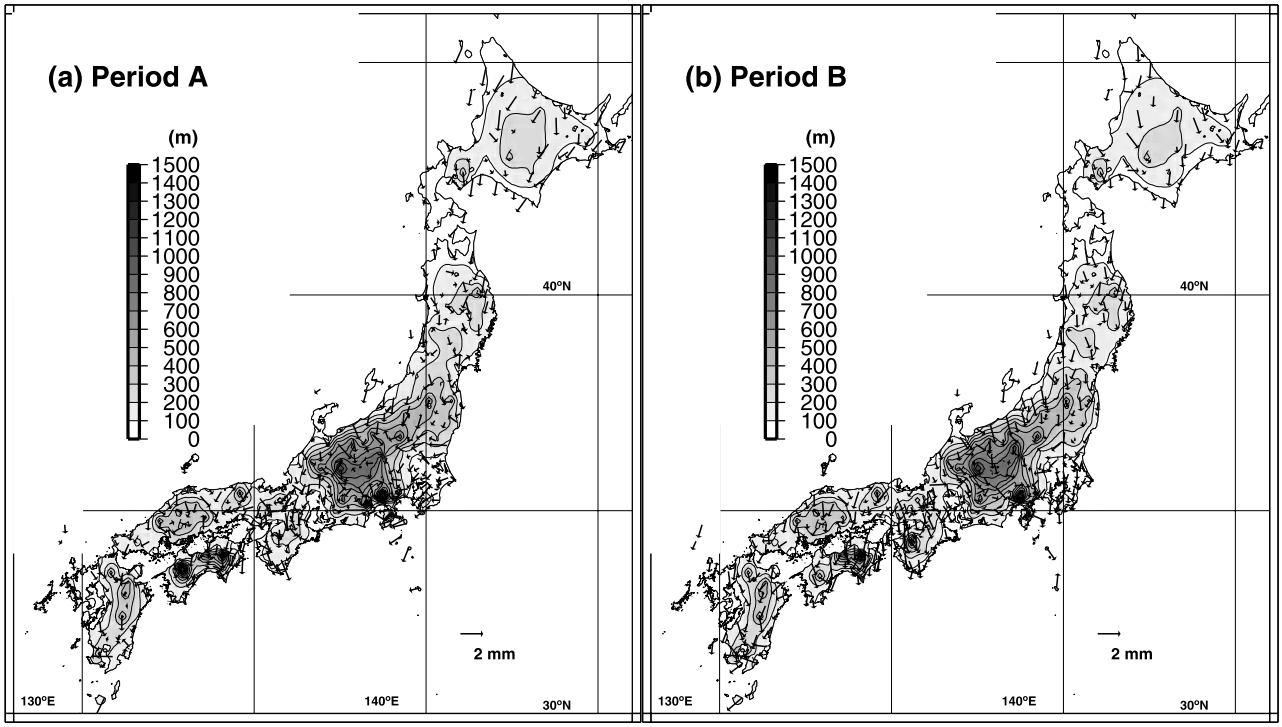


**Figure 7.** Spatial distribution of the tropospheric delay gradient vector averaged for the two periods, (a) Period A and (b) Period B, in Grad. The topographic height for GEONET is also plotted.

equal in magnitude to the ZTD difference caused by north tropospheric delay gradient of 1 mm, they depend on antenna-monument types. These systematic differences would be due to the azimuthal dependency in the PCV unmodeled in the GEONET PCV model. It is also unmodeled in IGS_01 model generally used in GPS analyses. Figure 6 also shows that daily averages for all sites in the north gradient have negative correlation with those in the ZTD differences. It is the same trend with correlations shown in Figure 5.

### 3.3. Reproduction of ZTD Biases Without Estimating Tropospheric Delay Gradient

[24] The relationship between the north component of the tropospheric delay gradient vectors and the ZTD differences (No-grad minus Grad) is reproduced by analyzing simulated data generated using GPSSIM, one of the programs (source code was slightly modified to enable applications of tropospheric delay gradients) in the Bernese software [*Rothacher and Mervart*, 1996] to synthesize GPS data. We assumed a virtual observation site in Mizusawa, Japan, at 39°N, and the ephemeris file on 8 March 1995, and generated 24-hour synthetic data assuming various elevation cutoff angles. We applied a fixed amount of north tropospheric gradient, and estimated the site coordinate and ZTD simultaneously paying no attention to tropospheric delay gradients. We found that the north tropospheric gradient affects not only the north position component but also the vertical component and ZTD estimates, depending on the cutoff angle of GPS satellites. For the cutoff angle of 15° in GEONET observation, north tropospheric delay gradient of 1 mm gave rise to the negative ZTD biases of about 1 mm, which is consistent with the tendency shown in Figure 5.

[25] Correlation between the north gradients and ZTD comes from the characteristic distribution of GPS satellites in the sky. Because the inclinations of the orbits of the GPS satellites are 55°N, there is always a void (directions where GPS satellites do not appear) in the northern (southern) sky at stations in the northern (southern) hemisphere, respectively. It is suggested that such north-south satellite distribution asymmetry gives rise to the biases in the vertical position and ZTD. It should be noted that it depends on the site latitudes to what extent the ZTD and vertical coordinate are biased, e.g., the bias disappears on the equator and at poles where satellite coverage is azimuthally symmetric. The influence of the north gradient on the north and vertical components of coordinate is discussed in more detail by *Miyazaki et al.* [2003].

[26] In this section, we compare ZTD in the three types of solutions, Net (network solution), No-grad (no-gradient point solution), and Grad (gradient point solution). First, we find systematic differences of ZTD of several mm between Net and No-grad, suggesting that Net has small systematic biases depending on each cluster. Second, we find systematic ZTD differences of a few millimeters, which depend on the magnitude of the north component of the gradient vector. Third, we show that ZTD biases without estimating gradient vectors, are ~1 mm when tropospheric delay gradient of 1 mm exists in the simulation studies. We thus show that the tropospheric delay gradient model improves the accuracy of ZTD, especially in weather conditions that have strong anisotropic distribution of water vapor such as in Case I and Case II.

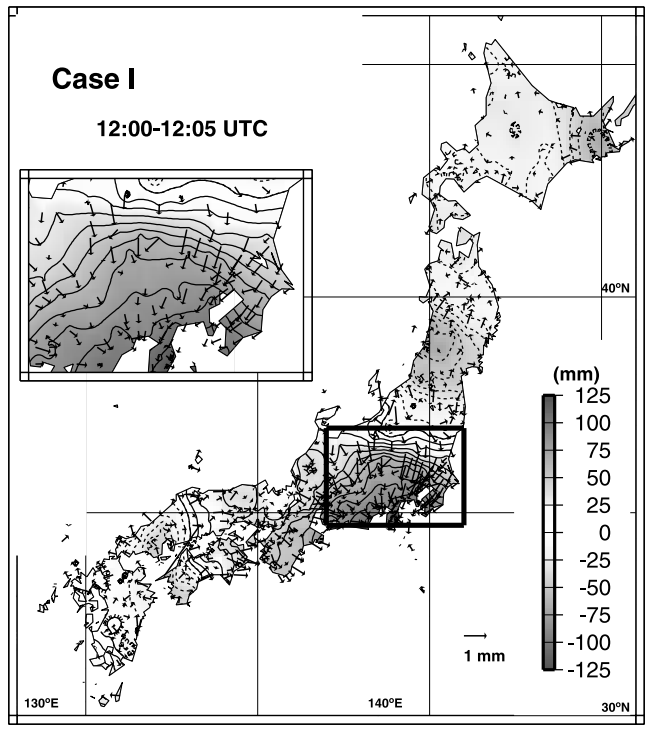


**Figure 8.** The relationship between horizontal gradient of the ZTD anomaly, $\nabla(\Delta ZTD(t))$, and anomalies of the tropospheric delay gradient anomaly, $\Delta\mathbf{G(t)}$, where two anomalies are computed by subtracting the averaged values for Period A from values estimated at 5-min intervals in Grad in Case I. The period used in Case I is from 1200 to 1205, 20 July (UTC). The region showing the significant and systematic correspondences between $\nabla(\Delta ZTD(t))$ and $\Delta\,\mathbf{G(t)}$ caused by the stationary tropical cyclone is enclosed with rectangles. See color version of this figure at back of this issue.

## 4. Behavior of Tropospheric Delay Gradients

[27] We have shown the importance of tropospheric delay gradients in the derivation of ZTD. However, other factors such as horizontal masks in mountainous areas may give rise to spurious tropospheric delay gradients, and here we examine if the estimated gradients reflect real atmospheric conditions. It is also important for meteorology to know if the gradient information including local structures of water vapor is usable for weather prediction. Figure 7 shows the spatial distribution of the averaged tropospheric delay gradient in the Grad for the two periods with the topographic height of GEONET (also refer to *Iwabuchi et al.* [2000], Plate 1). Most of the gradient vectors point southward, which is consistent with the Japanese climate, i.e., more water vapor in the south owing to higher temperatures. Positive systematic distributions of the ZTD difference for the 14-day periods in Figures 4a and 4b are also consistent with the simulation study because the 14-day averages of the estimated gradients generally point southward. The gradient of the atmospheric

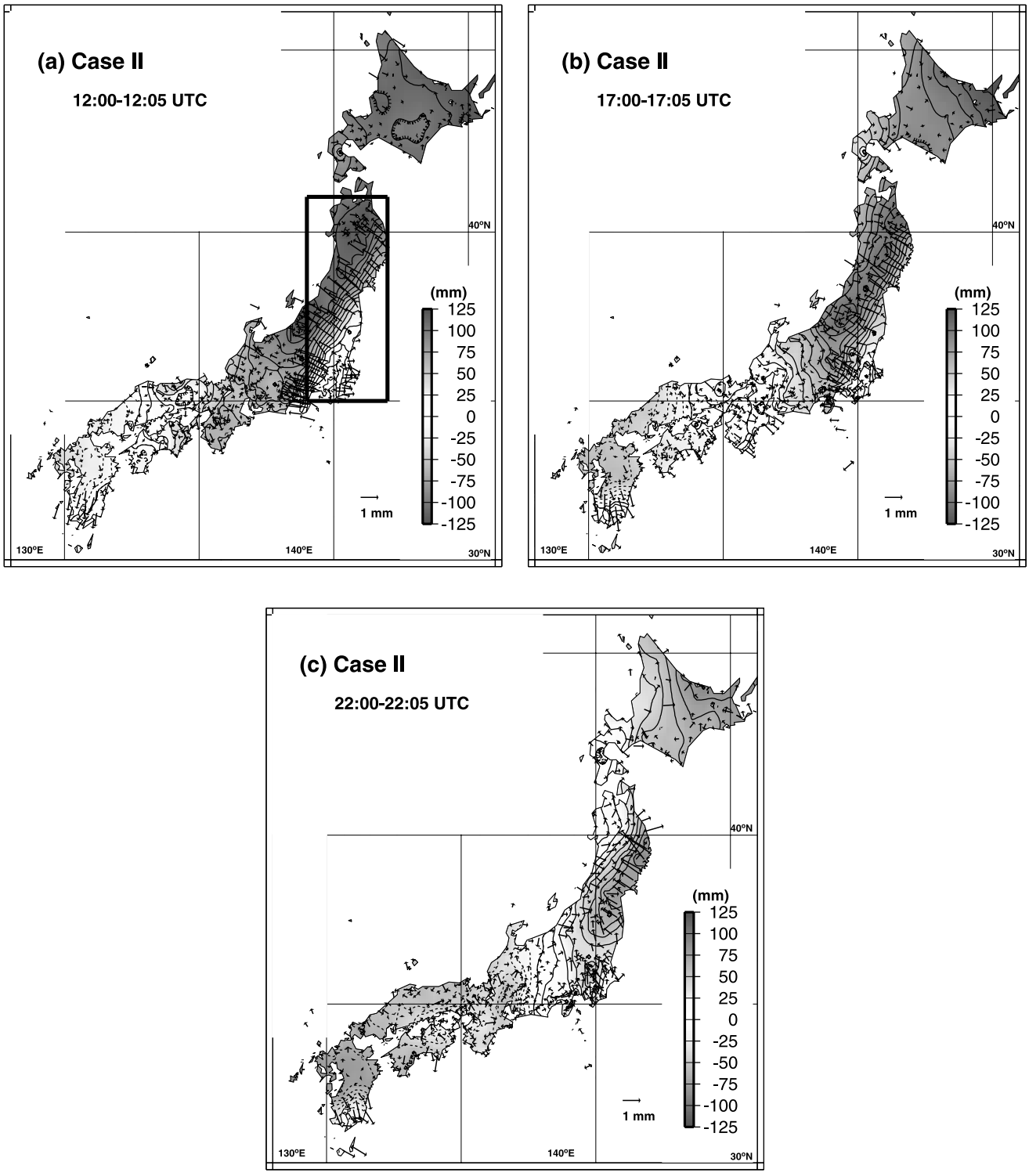


**Figure 9.** Same as Figure 8 but periods used in Case II are (a) from 1200 to 1205, (b) from 1700 to 1705, and (c) from 2200 to 2205 (UTC), 1 September, respectively. The region showing the significant and systematic correspondences between $\nabla(\Delta ZTD(t))$ and $\Delta\mathbf{G}(\mathbf{t})$ caused by the weather front is enclosed with rectangles. See color version of this figure at back of this issue.

pressure in summer may have partly contributed to these gradient vectors (in Japanese summer, atmospheric pressure tends to be higher in the southern region).

[28] We can see small differences between averaged tropospheric delay gradient vectors in Figures 7a and 7b. It may reflect a difference in the synoptic scale conditions of the weather, that is, seasonal variation of the water vapor distribution and atmospheric pressure. On the other hand, the averaged tropospheric delay gradient in Central Japan tend to climb toward the topographic high, especially in

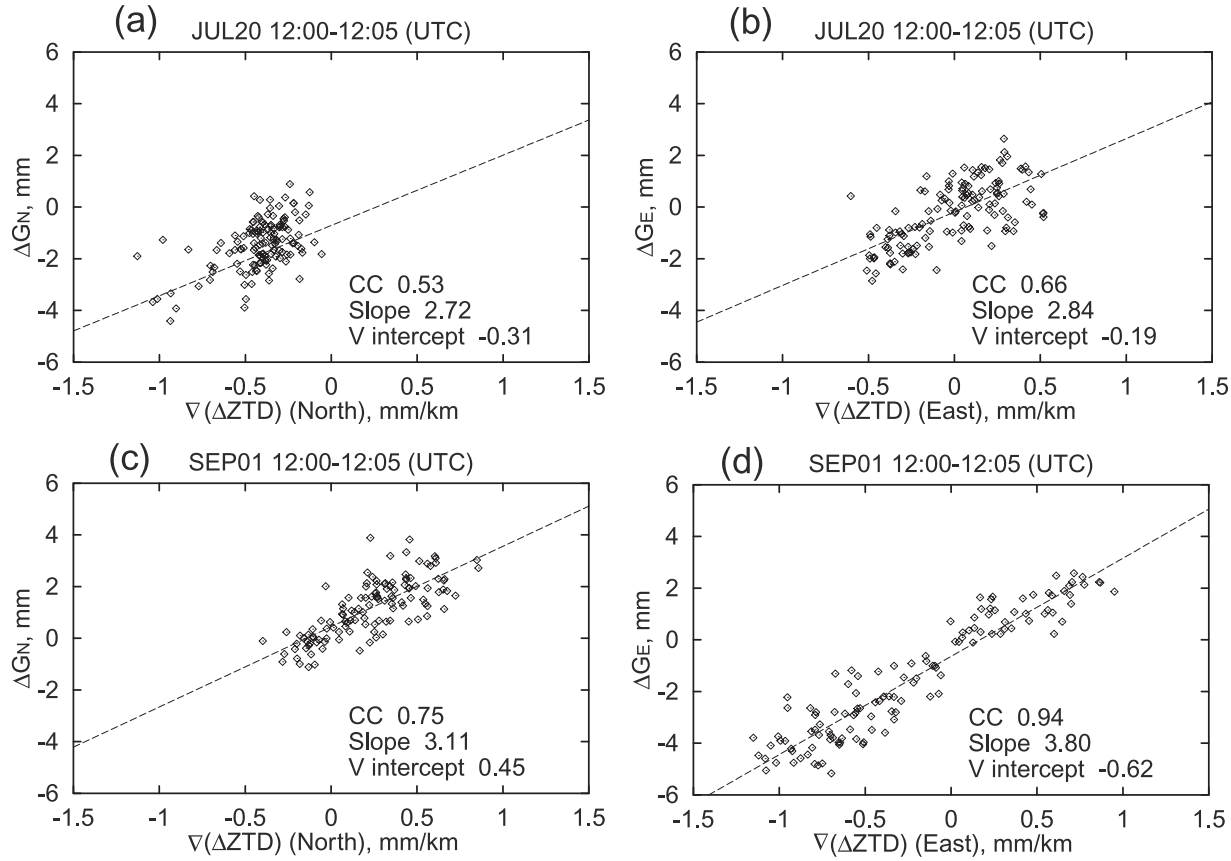


**Figure 10.** Correlation diagrams between magnitude of the horizontal gradient of the ZTD anomaly, $\nabla(\Delta ZTD(t))$, and magnitude of the tropospheric gradient anomaly in Grad for the north ($\Delta G_N$, left) and east ($\Delta G_E$, right) component from 1200 to 1205 UTC in Case I (top) and Case II (bottom) using the regions enclosed with rectangles on the maps in Figures 8 and 9, respectively. The correlation coefficient (CC) between the magnitude of the $\nabla(\Delta ZTD(t))$ and the magnitude of $\Delta\mathbf{G}(\mathbf{t})$, and slopes and vertical intercepts (V intercept) in the linear regression are displayed in the figure.

Period A. It may show that water vapor is distributed along the topographic contour in mountainous areas (rather than the equipotential surfaces) in summer when the westerlies are weak in Japan. The estimated tropospheric delay gradients may hence reflect water vapor trapped by topographic conditions at individual sites.

[29] Next we show the relationship between horizontal gradients of the ZTD distributions $\nabla ZTD$ and the tropospheric delay gradients, **G**, estimated in the point solution. The value $\nabla ZTD$ is known to be related to the tropospheric delay gradient vector as $\mathbf{G} = H \times \nabla ZTD$, where $H$ is the scale height of the atmosphere (and water vapor if the wet component is extracted) [e.g., *Ruffini et al.*, 1999]. This relationship provides information on the vertical profile of the water vapor, information useful for meteorological studies (it should be noted, however, that the gradient model assumes exponential decrease of water vapor with height [e.g., *Davis et al.*, 1993]). Here, we define ZTD anomaly, $\Delta ZTD(t)$ and gradient vector anomaly, $\Delta\mathbf{G}(t)$, showing temporal fluctuations of ZTD and **G** as

$$\Delta ZTD(t) = ZTD(t) - \overline{ZTD(t)} \tag{5}$$

$$\Delta\mathbf{G}(t) = \mathbf{G}(t) - \overline{\mathbf{G}(t)}, \tag{6}$$

where $\overline{ZTD(t)}$ and $\overline{\mathbf{G}(t)}$ represents temporal averages of $ZTD(t)$ and $\mathbf{G}(t)$ over the whole periods at each site, respectively. Since the component of high variability, mostly originating from water vapor, would be efficiently isolated by computing such anomalies, we call $\Delta ZTD(t)$ and $\Delta\mathbf{G}(t)$, "ZTD anomaly" and "gradient anomaly."

[30] Figure 8 shows the relationship between $\Delta ZTD(t)$ and $\Delta\mathbf{G}(t)$. Small contour intervals of $\Delta ZTD(t)$ show strong horizontal gradients in the ZTD distributions. The $\Delta\mathbf{G}(t)$ point to the regional ZTD maxima, or the center of the tropical cyclone and the weather front. Figure 9 shows temporal variations of $\Delta ZTD(t)$ and $\Delta\mathbf{G}(t)$ in 5-hour intervals in Case II. The $\Delta\mathbf{G}(t)$ are seen to follow the rapid variation of ZTD during the passage of the front along which $\Delta ZTD(t)$ are greater.

[31] Figure 10 shows the correlation diagrams between magnitudes of $\nabla(\Delta ZTD(t))$ and $\Delta\mathbf{G}(t)$ in Case I and Case II. In the figure, we use only sites in the regions enclosed by rectangles in Figures 8 and 9, where strong tropospheric delay gradient anomalies are seen. We calculated $\nabla(\Delta ZTD(t))$ at any points with the least squares method by interpolating using $\Delta ZTD(t)$ around the site. That is based on the method that *Shen et al.* [1996] used in their strain rate analysis. The effective radius for a site is 50 km. Correlations between the two types of gradients are confirmed

in north and south components; the correlation coefficients are 0.53 and 0.66 in Case I and 0.75 and 0.94 in Case II for north and east components, respectively. The correlation is very strong between $\nabla(\Delta ZTD(t))$ and $\Delta \mathbf{G}(t)$ in the east component of Case II. It possibly reflects systematic water vapor distribution caused by the weather front, suggesting that even the tropospheric gradients estimated in a severe weather condition are reliable. These results support the physical reality of the estimated tropospheric delay gradients and their usefulness for meteorological studies.

## 5. Summary

[32] We evaluated zenith tropospheric delays over the Japanese Islands in summer retrieved from the nationwide GPS array, GEONET, during two 14-day periods, and 2 days within them when a tropical cyclone and a weather front occurred. On both days, water vapor was very unevenly distributed. We were interested in the difference between the PWV derived by the GSI's network solution and the numerical weather prediction or radiosonde observations. For this purpose, we conducted a precise point positioning and compared the estimated ZTD with those obtained from the network solution. Systematic bias of several mm was found for the 14-day averaged ZTD. The difference was found to depend on the cluster in the network analysis, suggesting that the network solution has small systematic biases depending on each cluster.

[33] We then investigated the effect of a tropospheric delay gradient model in GPS analysis. Again we performed precise point positioning, enabling the option of tropospheric delay gradient estimation, and evaluated the ZTD differences between the two solutions, with and without the tropospheric delay gradient. Tropospheric delay gradient of 1 mm corresponded to $\sim$1 mm of the ZTD biases, which agreed with our simulation studies.

[34] Finally we investigated the reality of the estimated tropospheric delay gradients. Overall directions of the 14-day average of the gradient vectors point southward for both periods, which is consistent with the general summer climatic trend in Japan. We then showed that temporal fluctuations of the tropospheric delay gradients with respect to its 14-day average (gradient anomaly) changed directions rapidly, responding faithfully to the temporal variation of ZTD distributions. Those results suggest that the tropospheric delay gradient model works efficiently in the condition that water vapor distribution is highly azimuthally asymmetric. Estimated gradient reflects the real water vapor distribution.

[35] Throughout the present study, we evaluated tropospheric delays derived by GPS. We demonstrated that the tropospheric delay gradient model improves the accuracy of ZTD, but other aspects such as multipath, need to be investigated quantitatively in the future.

[36] **Acknowledgments.** We thank Ryu Ohtani (Geological Survey of Japan) for suggestions on data processing with GIPSY-OASIS II software. We especially thank two anonymous reviewers for their valuable comments to this study. A software package, Generic Mapping Tool (GMT), was used to plot the figures. This study is granted by GPS Meteorology Project of Japan of the Science and Technology Agency and by the Ministry of Education, Culture, and Sciences (grants 08640552 and 10559023).

## References

Askne, J., and H. Nordius, Estimation of tropospheric delay for microwave from surface weather data, *Radio Sci.*, *22*, 379–386, 1987.

Bar-Sever, Y. E., P. M. Kroger, and J. A. Borjesson, Estimating horizontal gradients of tropospheric path delay with a single GPS receiver, *J. Geophys. Res.*, *103*, 5019–5035, 1998.

Beutler, G., et al., *Bernese GPS software version 4.2*, 436 pp., Astron. Inst., Univ. of Berne, Berne, Switzerland, 2000.

Bevis, M., S. Businger, T. A. Herring, C. Rocken, R. A. Anthes, and R. H. Ware, GPS meteorology: Remote sensing of atmospheric water vapor using the Global Positioning System, *J. Geophys. Res.*, *97*, 15,787–15,801, 1992.

Businger, S., S. R. Chiswell, M. Bevis, J. Duan, R. A. Anthes, C. Rocken, R. H. Ware, M. Exner, T. Van Hove, and F. S. Solheim, The promise of GPS in atmospheric monitoring, *Bull. Am. Meteorol. Soc.*, *77*, 5–18, 1996.

Davis, J. L., T. A. Herring, I. I. Shapiro, A. E. E. Rogers, and G. Elgered, Geodesy by radio interferometry: Effects of atmospheric modeling errors on estimates of baseline length, *Radio Sci.*, *20*, 1593–1607, 1985.

Davis, J. L., G. Elgered, A. E. Niell, and C. E. Kuehn, Ground-based measurement of gradients in the "wet" radio refractive index of air, *Radio Sci.*, *28*, 1003–1018, 1993.

Duan, J., et al., GPS meteorology: Direct estimation of the absolute value of precipitable water, *J. Appl. Meteorol.*, *35*, 830–838, 1996.

Elosegui, P., J. L. Davis, R. T. K. Jaldehag, J. M. Johansson, A. E. Niell, and I. I. Shapiro, Geodesy using the Global Positioning System: The effects of signal scattering on estimates of site position, *J. Geophys. Res.*, *100*, 9921–9934, 1995.

Fang, P., M. Bevis, Y. Bock, S. Gutman, and D. Wolfe, GPS meteorology: Reducing systematic errors in geodetic estimates for zenith delay, *Geophys. Res. Lett.*, *25*, 3583–3596, 1998.

Georgiadou, Y., and A. Kleusberg, On carrier signal multipath effects in relative GPS positioning, *Manuscr. Geod.*, *13*, 172–179, 1998.

Hatanaka, Y., M. Sawada, A. Horita, and M. Kusaka, Calibration of antenna-radome and monument-multipath effect of GEONET, part 1, Measurement of phase characteristics, *Earth, Planets Space*, *53*, 13–21, 2001a.

Hatanaka, Y., M. Sawada, A. Horita, M. Kusaka, J. Johnson, and C. Rocken, Calibration of antenna-radome and monument-multipath effect of GEONET, part 2, Evaluation of the Phase Map by GEONET data, *Earth, Planets Space*, *53*, 23–30, 2001b.

Hatanaka, Y., A. Sengoku, T. Sato, J. M. Johnson, C. Rocken, and X. Meertens, Detection of tidal loading signals from GPS permanent array of GSI Japan, *J. Geod. Soc. Jpn.*, *47*, 187–192, 2001c.

Hogg, D. C., F. O. Guiraud, and M. T. Decker, Measurement of excess transmission length on Earth-space paths, *Astron. Astrophys.*, *95*, 304–307, 1981.

Iwabuchi, T., I. Naito, and N. Mannoji, A comparison of Global Positioning System retrieved precipitable water vapor with the numerical weather prediction analysis data over the Japanese Islands, *J. Geophys. Res.*, *105*, 4573–4585, 2000.

Kuo, Y.-H., X. Zou, and Y.-R. Guo, Variational assimilation of precipitable water using a nonhydrostatic mesoscale adjoint model, *Mon. Weather Rev.*, *124*, 122–147, 1996.

MacMillan, D. S., Atmospheric gradients from very long baseline observations, *Geophys. Res. Lett.*, *22*, 1041–1044, 1995.

Matsumoto, K., T. Sato, T. Takanezawa, and M. Ooe, GOTIC2: A program for comutation of oceanic tidal loading effect, *J. Geod. Soc. Jpn.*, *47*, 243–248, 2001.

Miyazaki, S., and K. Heki, Crustal velocity field of southwest Japan: Subduction and arc-arc collision, *J. Geophys. Res.*, *106*, 4305–4321, 2001.

Miyazaki, S., T. Saito, M. Sasaki, Y. Hatanaka, and Y. Imura, Expansion of GSI's nationwide GPS array, *Bull. of the Geographical Surv. Inst.*, *43*, 23–34, 1997.

Miyazaki, S., T. Iwabuchi, K. Heki, and I. Naito, An impact of estimating tropospheric gradient on precise positioning in summer using the Japanese nationwide GPS array, *J. Geophys. Res.*, *108*, doi:10.1029/2000JB000113, in press, 2003.

Naito, I., Y. Hatanaka, N. Mannoji, R. Ichikawa, S. Shimada, T. Yabuki, H. Tsuji, and T. Tanaka, Global Positioning System project to improve Japanese weather, earthquake prediction, *EOS Trans. Amer. Geophys. Union*, *79*, 301–311, 1998.

Niell, A. E., Global mapping functions for the atmosphere delay at radio wavelength, *J. Geophys. Res.*, *101*, 3227–3246, 1996.

Ohtani, R., and I. Naito, Comparisons of GPS derived precipitable water vapors with radiosonde observation in Japan, *J. Geophys. Res.*, *105*, 26,917–26,930, 2000.

Pondeca, M. S. F. V., and X. Zou, A case study of the variational assimilation of GPS zenith delay observations into a mesoscale model, *J. Appl. Meteorol.*, *40*, 1559–1576, 2001.

Rocken, C., R. Ware, T. Van Hove, F. Solheim, C. Alber, J. Johnson, M. Bevis, and S. Businger, Sensing atmospheric water vapor with the Global Positioning System, *Geophys. Res. Lett.*, *20*, 2631–2634, 1993.

Rocken, C., T. Van Hove, J. Johnson, F. Solheim, R. Ware, M. Bevis, S. Chiswell, and S. Businger, GPS/STORM-GPS sensing of atmospheric water vapor for meteorology, *J. Atmos. Oceanic Technol.*, *12*, 468–478, 1995.

Rothacher, M., and L. Mervart (Eds.), *Bernese GPS software version 4.0*, 418 pp., Astron. Inst., Univ. of Berne, Berne, Switzerland, 1996.

Ruffini, G., L. P. Kruse, A. Rius, B. Burki, L. Cucurull, and A. Flores, Estimation of tropospheric zenith delay and gradients over the Madrid area using GPS and WVR data, *Geophys. Res. Lett.*, *26*, 447–450, 1999.

Shen, Z.-K., D. D. Jackson, and B. X. Ge, Crustal deformation across and beyond the Los Angeles basin from geodetic measurements, *J. Geophys. Res.*, *102*, 27,957–27,980, 1996.

Schupler, B. R., R. L. Allhouse, and T. A. Clark, Signal characteristics of GPS user antennas, *Navigation*, *41*, 277–295, 1994.

Tregoning, P., R. Boers, D. O'Brien, and M. Hendy, Accuracy of absolute precipitable water vapor estimates from GPS observations, *J. Geophys. Res.*, *103*, 28,701–28,710, 1998.

Tsuda, T., et al., GPS meteorology project of Japan—Exploring frontiers of geodesy, *Earth, Planets Space*, *50*, i–v, 1998.

Ware, R., et al., GPS sounding of the atmosphere from low Earth orbit: Preliminary results, *Bull. Am. Meteorol. Soc.*, *77*, 19–40, 1996.

Ware, R. H., D. W. Fulker, S. A. Stein, D. N. Anderson, S. K. Avery, R. D. Clark, K. K. Droegemeier, J. P. Kuettner, J. B. Minster, and S. Sorooshian, SuomiNet: A real-time national GPS network for atmospheric research and education, *Bull. Am. Meteorol. Soc.*, *81*, 677–694, 2000.

Zumberge, J. F., M. B. Heflin, D. C. Jefferson, M. M. Watkins, and F. H. Webb, Precise point positioning for the efficient and robust analysis of GPS data from large networks, *J. Geophys. Res.*, *102*, 5005–5017, 1997.

Y. Hatanaka, Geodetic Observation Center, Geographical Survey Institute, Kitasato 1, Tsukuba, Japan. (hata@gsi.go.jp)

K. Heki, Division of Earth Rotation, National Astronomical Observatory, Mizusawa, Iwate, 023-0861, Japan. (heki@miz.nao.ac.jp)

T. Iwabuchi, The Forecast Research Department, Meteorological Research Institute, Nagamine 1-1, Tsukuba, 305-0052, Japan. (iwabuch@ucar.edu)

S. Miyazaki, Earthquake Research Institute, University of Tokyo, 1-1, Yayoi-1, Bunkyo-ku, Tokyo, 113-0032, Japan. (miyazaki@eri.u-tokyo.ac.jp)

I. Naito, Division of Earth Rotation, National Astronomical Observatory, Osawa 2-21-1, Mitaka, Tokyo, 181-8588, Japan. (naito.isao@nao.ac.jp)

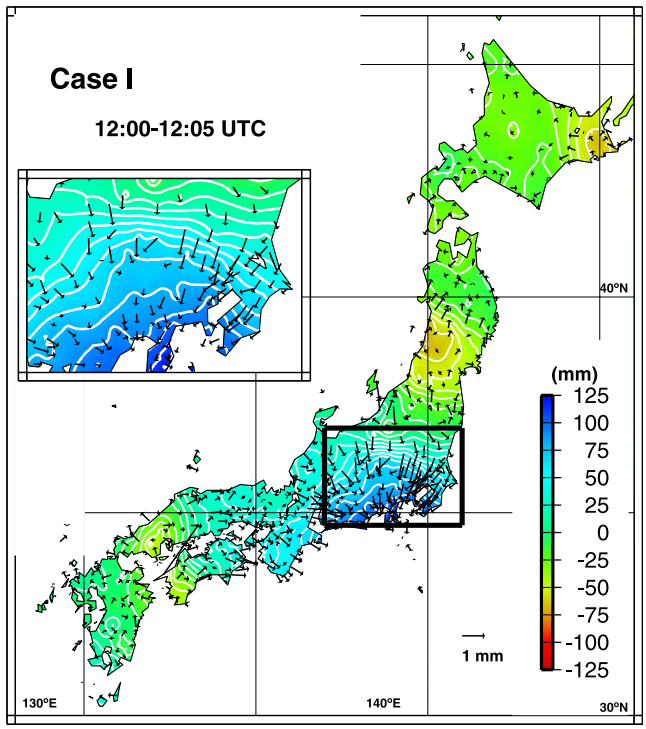


**Figure 8.** The relationship between horizontal gradient of the ZTD anomaly, $\nabla(\Delta ZTD(t))$, and anomalies of the tropospheric delay gradient anomaly, $\Delta\mathbf{G(t)}$, where two anomalies are computed by subtracting the averaged values for Period A from values estimated at 5-min intervals in Grad in Case I. The period used in Case I is from 1200 to 1205, 20 July (UTC). The region showing the significant and systematic correspondences between $\nabla(\Delta ZTD(t))$ and $\Delta$ **G(t)** caused by the stationary tropical cyclone is enclosed with rectangles.

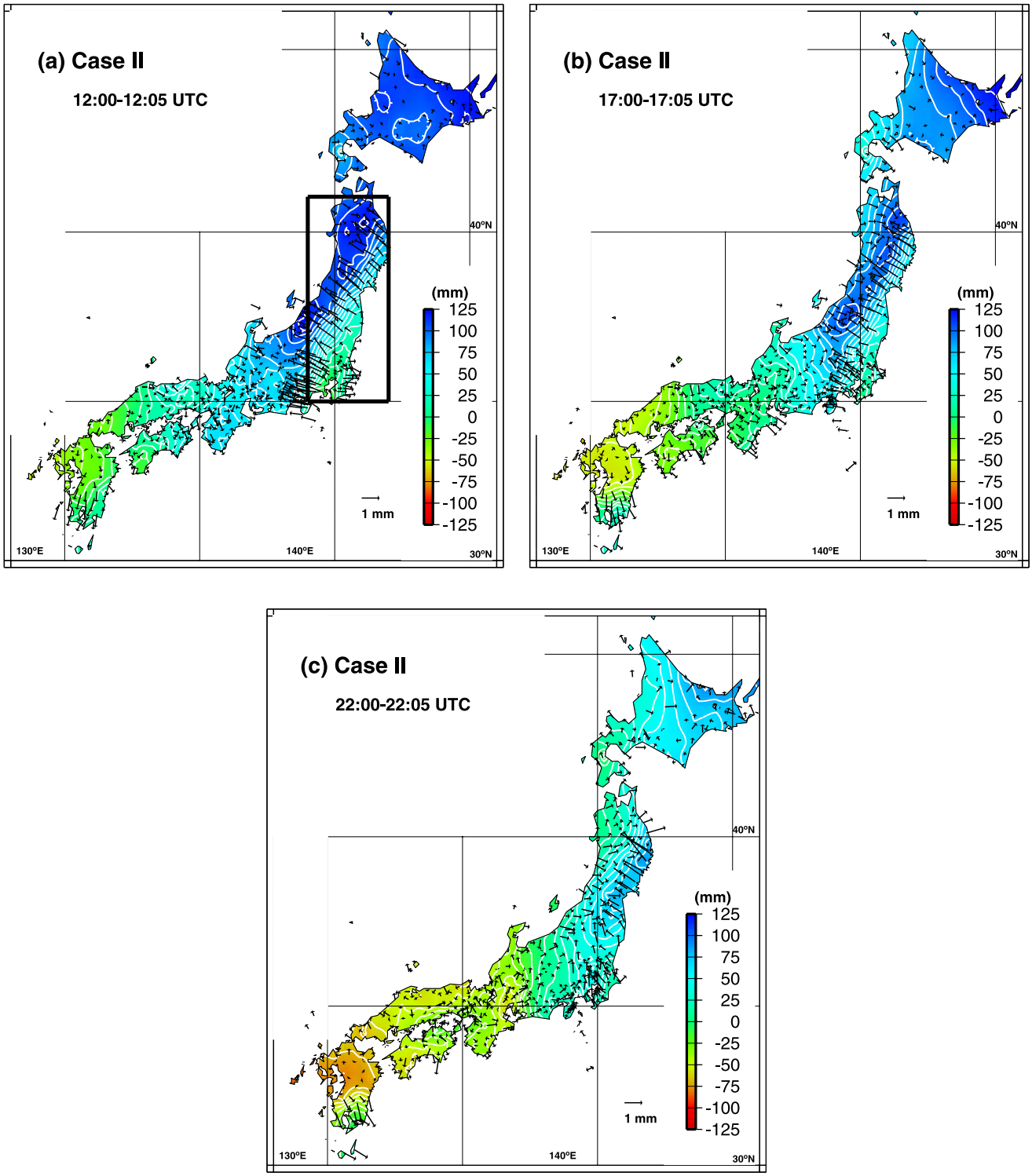


**Figure 9.** Same as Figure 8 but periods used in Case II are (a) from 1200 to 1205, (b) from 1700 to 1705, and (c) from 2200 to 2205 (UTC), 1 September, respectively. The region showing the significant and systematic correspondences between $\nabla(\Delta ZTD(t))$ and $\Delta\mathbf{G}(\mathbf{t})$ caused by the weather front is enclosed with rectangles.